Localization Effects on Magnetotransport of a Disordered Weyl Semimetal

E. Khalaf[1] and P. M. Ostrovsky[1,2]
[1]Max Planck Institute for Solid State Research, Heisenbergstrasse 1, 70569 Stuttgart, Germany
[2]L. D. Landau Institute for Theoretical Physics, 142432 Chernogolovka, Russia
(Received 10 December 2016; published 8 September 2017)

We study longitudinal magnetotransport in a disordered Weyl semimetal taking into account localization effects in the vicinity of a Weyl node exactly. In a magnetic field, a single chiral Landau level coexists with a number of conventional nonchiral levels. Disorder scattering mixes these topologically different modes leading to very strong localization effects. We derive the average conductance as well as the full distribution function of transmission probabilities along the field direction. Remarkably, we find that localization of the nonchiral modes is greatly enhanced in a strong magnetic field with the typical localization length scaling as $1/B$. Technically, we use the nonlinear sigma-model formalism with a topological term describing the chiral states. The problem is solved exactly by mapping to an equivalent transfer matrix Hamiltonian.

DOI: 10.1103/PhysRevLett.119.106601

Introduction.—Weyl semimetals have received considerable interest in the past years due to their unusual transport properties and exotic surface states [1–13]. A Weyl semimetal (WSM) is a three-dimensional (3D) analog of graphene characterized by the existence of isolated touching points between valence and conduction bands with linear electron dispersion. Each band touching point has a definite chirality and can be viewed as a magnetic monopole (source or sink of Berry flux) in momentum space. The topological nature of such Weyl points protects their linear spectrum from gap opening and significantly alters transport properties of the material compared to usual metals.

One immediate manifestation of the topological nature of the WSM spectrum is provided by the structure of Landau levels in an external magnetic field. Electron motion is confined in the plane perpendicular to the field yielding discrete energy levels

$$E_n = \hbar v \begin{cases} \mathrm{sgn} n \sqrt{4\pi |nB|/\Phi_0 + k_x^2}, & n \neq 0, \\ k_x, & n = 0. \end{cases} \quad (1)$$

Here, v is the Fermi velocity characterizing linear dispersion at the Weyl node and $\Phi_0 = hc/e$ is the magnetic flux quantum. Each discrete level has a macroscopic degeneracy $m = BA/\Phi_0$, where A is the total sample cross-section area. Landau level dispersion is illustrated in Fig. 1. The topological property of the Weyl point is manifested by a single unidirectional (chiral) level with $n = 0$, in addition to many nonchiral levels ($n \neq 0$). A chiral level propagating in the opposite direction belongs to another Weyl node and is well separated in the momentum space. This results in a very large negative magnetoresistance in the direction parallel to the field [12,14–17].

Despite the number of theoretical works discussing transport in a WSM [3,18–26], effects of disorder have not been taken into account beyond the semiclassical weak localization regime so far. This is justified in the absence of magnetic field since the material is three dimensional and localization effects are weak. For magnetotransport, the situation is drastically different. Since Landau levels disperse only along the field, electron transport is effectively quasi-one-dimensional (1D) [25] and hence subject to strong localization effects.

Scattering on impurities eventually localizes the nonchiral modes of the spectrum, while the chiral level evades localization. This protected chiral Landau level is the primary source of strong magnetoresistance. Backscattering of chiral states is only possible when impurities couple different Weyl nodes of opposite chirality, which occurs at parametrically larger length scales compared to the mean free path within each node.

In this Letter, we study transport in a generic quasi-1D system which hosts both chiral and nonchiral modes fully taking into account localization effects. Scattering on impurities eventually localizes the nonchiral modes, while the chiral level evades localization. This model describes

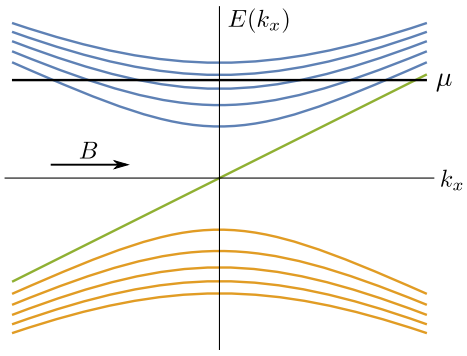

FIG. 1. The Landau levels in the vicinity of a Weyl point in the magnetic field B. The levels are nondispersive in the plane transverse to the magnetic field. The energy-momentum dependence along the field [Eq. (1)] is displayed. Each level has a macroscopic degeneracy $m = BA/\Phi_0$. The system is effectively a quasi-1D wire with both chiral and nonchiral channels provided $L \gg \sqrt{A}$.

 © 2017 American Physical Society

longitudinal magnetotransport in a WSM at finite doping with some fixed nonzero chemical potential (cf. Fig. 1). For a WSM sample with macroscopic length L and cross section A, quasi-1D geometry means $L \gg \sqrt{A}$. The surface states are ignored since their contribution to transport is negligible in a bulk sample [27].

We will show that, in the presence of m chiral channels, the typical localization length for nonchiral modes is significantly reduced, $\xi^{\mathrm{typ}} = \xi/(1+m)$. Here $\xi = \sigma A$ is the localization length the system would have in the absence of chiral modes, σ is the 3D conductivity (in units e^2/h per Weyl node) given by the product of electron charge, density of states, and diffusion constant $D = vl$. For magnetotransport in a WSM with a macroscopic degeneracy of the chiral Landau level $m = BA/\Phi_0 \gg 1$, the typical localization length for nonchiral modes $\xi^{\mathrm{typ}} = \sigma\Phi_0/B$ is independent of A. This effectively 1D localization effect is so strong that it can be observed in a WSM sample of arbitrary thickness. The enhancement of localization of the nonchiral channels can be understood in terms of statistical level repulsion between the transmission eigenvalues in the system, where the presence of chiral channels with perfect transmission suppresses transport from the remaining nonchiral ones.

Aside from magnetotransport in a WSM, a quasi-1D wire model with chiral channels applies to a number of other systems such as the interface between two quantum Hall samples [28–32] and graphene zigzag nanoribbons [33]. We obtain closed analytic expressions for the conductance as a function of L, disorder strength, and number of chiral channels taking into account localization effects exactly. In addition, we also consider the distribution function of transmission eigenvalues [34,35], that contains information about shot noise and other higher moments of full-counting statistics [35–37].

Formalism.—We consider a model of a quasi-1D wire of length L attached to two leads with $N \gg 1$ channels in total and imbalance m (difference of right- and left-propagating modes). Disorder mixes all channels at the scale of the mean free path l. The full information about electron transport is captured by the distribution function of N transmission probabilities which we will explicitly derive.

The main technical tool we use to describe the disordered system is the supermatrix nonlinear sigma model [32,38–40]. It can be derived following the conventional procedure [38–40] starting from the effective action for the noninteracting electrons, averaging over disorder potential, decoupling of the fields with the help of Hubbard-Stratonovich transformation (that introduces the matrix Q). Integrating out the original electron fields, and performing the gradient expansion at the saddle-point manifold yields the sigma model action [25,32]

$$S[Q] = -\int_0^L dx \mathrm{str}\left[\frac{\xi}{8}\left(\frac{\partial Q}{\partial x}\right)^2 + \frac{m}{2}T^{-1}\Lambda\frac{\partial T}{\partial x}\right],$$
$$\xi = Nl = \sigma A, \quad Q = T^{-1}\Lambda T, \quad \Lambda = \mathrm{diag}(1,-1)_{\mathrm{RA}}. \tag{2}$$

The field Q is a 4×4 supermatrix operating in the product of retarded-advanced (RA) space and the Bose-Fermi superspace (BF). The supertrace "str" is defined by $\mathrm{str}A = \mathrm{tr}A_{\mathrm{BB}} - \mathrm{tr}A_{\mathrm{FF}}$ as in Ref. [40].

The sigma model Eq. (2) describes magnetotransport in a WSM in the vicinity of a single Weyl node. The effect of the coupling between different nodes will be discussed later.

The matrix Q obeys the nonlinear constraint $Q^2 = 1$ and can be parametrized in terms of the unitary supermatrix T as indicated in Eq. (2). The matrix Q is invariant under the gauge transformation $T \mapsto KT$ for any matrix K that commutes with Λ. However, the second term of the action Eq. (2) is written as a functional of T rather than Q and changes by an integral of the total derivative $(m/2)\partial_x \mathrm{str}(\Lambda \ln K)$ under such a transformation. The reason for this is that the theory Eq. (2) describes a single Weyl node. The gauge invariance is restored when a Weyl node of opposite chirality is included. It is worth noting that this second term naturally appears in the field theory of a quantum Hall edge [41] and constitutes a 1D version of the Wess-Zumino-Witten term [42–44].

In order to access transport characteristics of the system, we apply twisted boundary conditions with the counting field introduced by Nazarov [32,35,45]

$$Q(0) = \Lambda, \qquad Q(L) = \begin{pmatrix} \cos\hat{\theta} & \sin\hat{\theta} \\ \sin\hat{\theta} & -\cos\hat{\theta} \end{pmatrix}_{\mathrm{RA}}, \tag{3}$$

where $\hat{\theta} = \mathrm{diag}(i\theta_B, \theta_F)_{\mathrm{BF}}$. The transmission distribution function can be obtained from the partition function of the sigma model as [46]

$$\psi(\theta_B, \theta_F) = \int_{Q(0)}^{Q(L)} DQ e^{-S[Q]}, \tag{4}$$

$$\rho(\lambda) = -\frac{2}{\pi}\mathrm{Re}\frac{\partial}{\partial\theta_F}\psi(\theta_B,\theta_F)\Big|_{i\theta_B=\theta_F=\pi+2i\lambda-0}. \tag{5}$$

The function $\rho(\lambda)$ is the probability density for the Lyapunov exponent λ related to the transmission probability by $T = \cosh^{-2}\lambda$ [32,35,47]. It can be used to compute any moment of the full counting statistics. In this work, we are particularly interested in the average conductance per Weyl node (measured in units of e^2/h)

$$G = \int_0^\infty \frac{d\lambda\rho(\lambda)}{\cosh^2\lambda} = -2\frac{\partial^2}{\partial\theta_F^2}\psi(\theta_B,\theta_F)\Big|_{\theta_B=\theta_F=0}, \tag{6}$$

Transfer matrix Hamiltonian.—The path integral Eq. (4) can be computed analytically by mapping to the equivalent Schrödinger equation with the position x playing the role of fictitious imaginary time [38,39,48]

$$\xi\frac{\partial\psi}{\partial x} = -\mathcal{H}\psi. \tag{7}$$

The action Eq. (2) describes the motion of a particle on the curved supermanifold parametrized by the matrix Q. The

presence of chiral modes (second term of the action) results in an effective uniform magnetic field across the manifold with the vector potential $A=-(m/2)\mathrm{str}(T^{-1}\Lambda dT)$. As a result, the transfer matrix Hamiltonian is given by the Laplace-Beltrami operator on the supermanifold with the long derivatives $\partial \mapsto \partial + A$ [46].

The initial conditions (at $x=0$) force the wave function to be unity at $Q=\Lambda$ and zero everywhere else, see Eq. (3). Such a function is invariant under rotating $Q \mapsto K^{-1}QK$ by any matrix K that commutes with Λ. This symmetry is preserved by the Hamiltonian $\mathcal{H}$ provided that we compensate the rotation by a gauge transformation: $T \mapsto K^{-1}TK$. As a result, the Hamiltonian conserves the angular momentum corresponding to K rotations and can be restricted to the zero angular momentum sector: $\psi(K^{-1}QK)=\psi(Q)$ at every x. Such functions are parametrized by just two polar angles $0 \le \theta_F \le \pi$ and $\theta_B \ge 0$ as in Eq. (3). The details of the parametrization and the gauge choice can be found in Supplemental Material [46]. The explicit effective Hamiltonian has the form

$$\mathcal{H}=-\frac{1}{J}\frac{\partial}{\partial\theta_F}J\frac{\partial}{\partial\theta_F}-\frac{1}{J}\frac{\partial}{\partial\theta_B}J\frac{\partial}{\partial\theta_B}+\frac{m^2}{4}V(\theta_B,\theta_F),$$
$$J=\frac{\sin\theta_F\sinh\theta_B}{(\cosh\theta_B-\cos\theta_F)^2},\quad V=\cos^{-2}\frac{\theta_F}{2}-\cosh^{-2}\frac{\theta_B}{2}. \tag{8}$$

Eigenfunctions.—The Hamiltonian Eq. (8) can be diagonalized with the help of the Sutherland transformation $\tilde{\mathcal{H}}=J^{1/2}\mathcal{H}J^{-1/2}=\tilde{\mathcal{H}}_F+\tilde{\mathcal{H}}_B$ which decouples the variables θ_B and θ_F [45,46,49]. The eigenvalues of $\tilde{\mathcal{H}}_F$ form a discrete spectrum with the lowest eigenvalue $(m+1)^2/4$. The spectrum of $\tilde{\mathcal{H}}_B$ is continuous above zero supplemented by a discrete set of negative eigenvalues (unless $m=0$) with the lowest at $-(m-1)^2/4$. The overall lowest eigenvalue of $\tilde{\mathcal{H}}$ is $1/4$ in the case $m=0$, otherwise it equals m. The analysis of the full spectrum with the explicit form of the normalized eigenfunctions can be found in Supplemental Material [46].

Once the eigenfunctions ϕ_ν of the transfer matrix Hamiltonian and the corresponding eigenvalues ϵ_ν are known, the solution to the time-evolution problem Eq. (7) can be written explicitly as a spectral expansion [45,50,51]

$$\psi(\theta_B,\theta_F,x)=\frac{\cos^m(\theta_F/2)}{\cosh^m(\theta_B/2)}+\sum_\nu \phi_\nu(\theta_B,\theta_F)e^{-(x/\xi)\epsilon_\nu}. \tag{9}$$

Here the sum over ν implies a sum over discrete levels and an integral over the continuous part of the spectrum. The eigenfunctions are normalized such that the initial condition is satisfied.

The first term in Eq. (9) is the ground state of the transfer matrix Hamiltonian $\mathcal{H}$ with zero eigenvalue. Its contribution to the function ψ and hence to all transport quantities is independent of the length x. This zero eigenfunction encodes the effect of chiral topologically protected channels and contributes $me^2/2h$ to the average conductance. The rest of the spectrum is separated by a finite gap from the ground state and describes the effect of the remaining nonchiral modes. Exponential decay of the second term in Eq. (9) signifies localization of the unprotected channels with the gap setting the value of the corresponding localization length $\sim\xi/m$.

Results.—The distribution function $\rho(\lambda)$ is computed from ψ at $x=L$ using Eq. (5). The result has the form

$$\rho(\lambda)=m\delta(\lambda)+\frac{\sinh 2\lambda}{\pi}\sum_{l\in 2\mathbb{N}+1+m}\int_{-\infty}^{\infty}dr\,\frac{lre^{-\frac{L}{4\xi}(l^2+r^2)}}{l^2+r^2}$$
$$\times\sinh\frac{\pi}{2}(r-im)P^{(-m,0)}_{\frac{ir+m-1}{2}}(\cosh 2\lambda)P^{(0,m)}_{\frac{l-m-1}{2}}(-\cosh 2\lambda). \tag{10}$$

Here $\mathbb{N}=0,1,\ldots$ and $P^{(\alpha,\beta)}_\nu(x)$ is the Jacobi polynomial of (possibly complex) order ν [46]. The term $m\delta(\lambda)$ represents the contribution of m chiral channels with ideal transparency.

The distribution function Eq. (10) is plotted in Fig. 2 for several values of m and L/ξ. Qualitatively, we observe (i) a suppression of the distribution close to $\lambda=0$ (which corresponds to ideal transmission) and (ii) "crystallization" of individual transmission eigenvalues in the limit $L\gg\xi$ [52,53]. Both effects can be interpreted in terms of statistical level repulsion. Different Lyapunov exponents λ repel each other with strength proportional to L/ξ. The presence of m eigenvalues pinned at $\lambda=0$ pushes the remaining spectrum away from zero.

In the limit $L\gg\xi$, the distribution function is a sum of equidistant Gaussian peaks with width $\sqrt{L/\xi}$ separated by L/ξ and having a unit weight. The position of the first peak determines the localization length governing the typical conductance (of nonchiral modes) $G_{\mathrm{typ}}=e^{\langle\ln G\rangle}\propto e^{-(L/\xi)(m+1)}$ leading to $\xi^{\mathrm{typ}}=\xi/(1+m)$.

The average conductance per Weyl node is given by Eq. (6) (in units of e^2/h)

$$G=\frac{m}{2}+\sum_{l\in 2\mathbb{N}+1+m}\int_{-\infty-im}^{\infty-im}dr\,\frac{lr\tanh\frac{\pi}{2}(r+im)}{l^2+r^2}e^{-\frac{L}{4\xi}(l^2+r^2)}. \tag{11}$$

It is shown in Fig. 3 as a function of L/ξ for different values of m. A smooth crossover from the diffusive limit $L\ll\xi$ to the strongly localized regime $L\gg\xi$ where current is carried only by the protected chiral channels is clearly visible. In the latter case, the conductance is given by

$$G=\frac{m}{2}+\begin{cases}2(\pi\xi/L)^{3/2}e^{-L/4\xi}, & m=0,\\ 2\sqrt{\xi/\pi L}e^{-L/\xi}, & m=1,\\ \frac{m^2-1}{m}e^{-mL/\xi}, & m\ge 2.\end{cases} \tag{12}$$

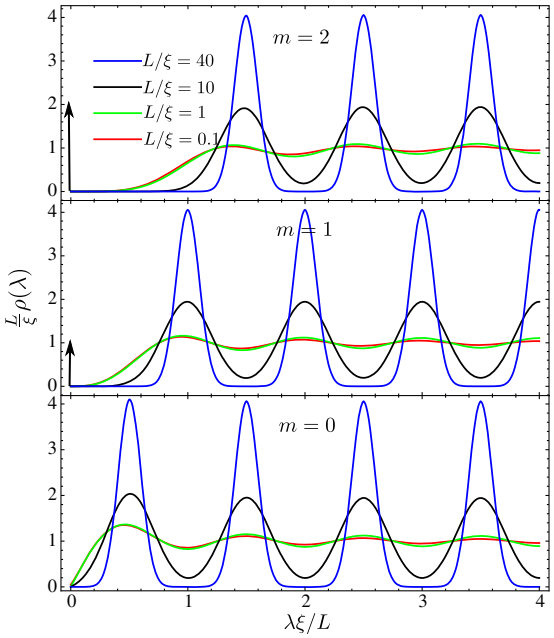

FIG. 2. Transmission distribution function $\rho(\lambda)$ for several values of m and L/ξ. The presence of m chiral channels depletes the distribution in the vicinity of $\lambda = 0$. Level "crystallization" occurs at $L \gg \xi$.

The localization length governing the decay of the average conductance (for the nonchiral modes) is generally different from the typical localization length [54]. For $m \neq 0$, it is significantly reduced: $\xi^{\mathrm{av}} = \xi/4m$.

Let us now discuss the longitudinal magnetoconductance of a WSM sample with length $L \ll \xi = \sigma A$. The magnetic field is directly related to the parameter $m = BA/\Phi_0$ (here B is the component of magnetic field in the direction of current). A crossover from quadratic to linear magnetoconductance occurs when B exceeds $B_c = 2\Phi_0\xi/LA = 2\sigma\Phi_0/L$. It corresponds to $m = \xi/L \gg 1$;

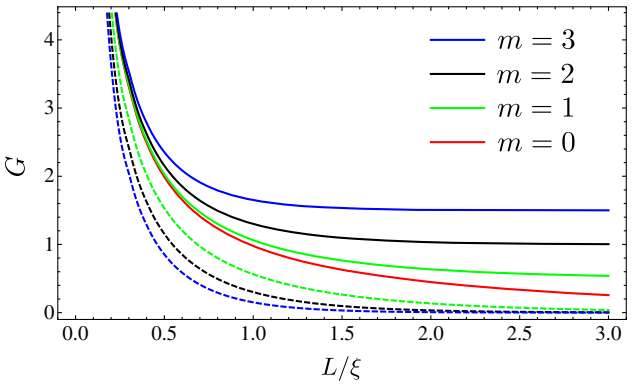

FIG. 3. Average conductance for different values of m as a function of L/ξ (solid) and the contribution of the nonchiral modes $G - G_\infty$ (dashed lines). For $L \ll \xi$, the behavior is metallic $G \sim \xi/L$, receiving contribution from all channels. For $L \gg \xi$, the conductance is solely due to the chiral channels and approaches $me^2/2h$.

hence, discreteness of m can be disregarded. The field B_c decreases with increasing disorder strength. In this limit, the magnetoconductance (Fig. 4) reduces to the semiclassical result [25,32]:

$$\frac{G(B)}{G(0)} = \frac{B}{B_c}\coth\frac{B}{B_c}. \tag{13}$$

Discussion.—In the presence of chiral channels, localization effects in the nonchiral bands are so strong that they can be observed in a 3D WSM sample. Both the length $\xi = \sigma A$ and the Landau level degeneracy $m = BA/\Phi_0$ scale linear with A. Hence the typical localization length $\xi^{\mathrm{typ}} = \sigma\Phi_0/B$ for the nonchiral modes remains finite for arbitrary sample cross section.

In a field stronger than $B_c = 2\sigma\Phi_0/L$, all the nonchiral modes are effectively localized and the current is carried only by the chiral channels representing the lowest Landau level. The value of B_c is considerably smaller than the ultraquantum field $B_u = (\mu/\hbar v)^2\Phi_0/4\pi$ at which only the lowest Landau level lies below the Fermi energy μ. Both B_c and B_u scale as μ^2 and their ratio is $B_c/B_u \sim l/L \ll 1$. This implies that the ultraquantum limit for transport in a disordered WSM occurs at much weaker fields than in the ideal clean material. The main experimental manifestation of this effect would be observing a linear longitudinal magnetoconductance coexisting with quantum oscillations indicating multiple Landau levels at the Fermi surface.

Our results are valid as long as scattering between different Weyl nodes is neglected. This is the case when the dominant scatterers are smooth on the scale of the lattice spacing and the Weyl nodes are well-separated in momentum space. Coupling between the Weyl nodes (e.g. by sharp impurities) introduces a length scale l_i. The effect of introducing this length scale would be replacing the sample length L with l_i in our results for magnetoconductivity. In particular, Eq. (13) reproduces the quadratic B dependence obtained from the kinetic equation treatment [18] in the limit of small B. The transport ultraquantum field is in this case related to the clean ultraquantum field

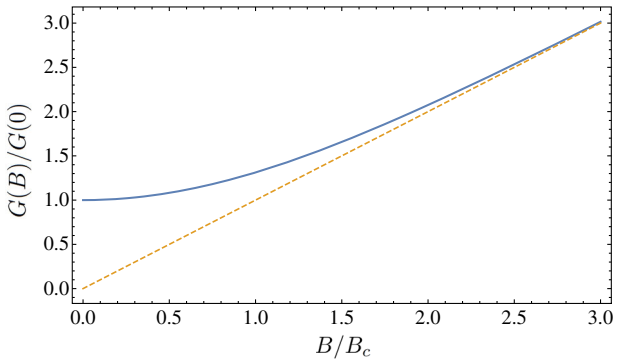

FIG. 4. Average magnetoconductance in the limit $L \ll \xi$. A crossover from quadratic to linear field dependence occurs at $B_c = 2\Phi_0\xi/LA = 2\sigma\Phi_0/L$.

by $B_c/B_u \sim l/l_i$ which is small for sufficiently smooth disorder [55].

Conclusion.—We have derived exact expressions for longitudinal conductance, Eq. (11), and transmission distribution function, Eq. (10), in a Weyl semimetal subject to an external magnetic field. The presence of the chiral topologically protected Landau level with the macroscopic degeneracy $m = BA/\Phi_0$ leads to a very efficient localization of the nonchiral states. An effective ultraquantum regime, where only the chiral modes contribute to transport, occurs at a length scale $\xi^{\mathrm{typ}} \approx \xi/m = \sigma\Phi_0/B$, see Fig. 3. Magnetoconductance changes from quadratic to linear at the disorder-dependent scale $B_c = 2\sigma\Phi_0/L$, Fig. 4, that is significantly smaller than the ultraquantum field for a clean sample, $B_c/B_u \sim l/L \ll 1$. Thus the magnetic field dramatically enhances disorder effects.

The same results apply in general to any quasi-1D system with broken time-reversal symmetry with a number of chiral modes m. The transmission distribution function, Fig. 2, interpolates between diffusive ($L \ll \xi$) and strongly localized ($L \gg \xi$) limits exhibiting "crystallization" of the Lyapunov exponents in the latter case. This effect can be interpreted in terms of statistical level repulsion.

We are grateful to D. Bagrets, A. Mirlin, M. Skvortsov, and A. Stern for valuable and stimulating discussions. The work was supported by the Russian Science Foundation (Grant No. 14-42-00044).

[1] X. Wan, A. M. Turner, A. Vishwanath, and S. Y. Savrasov, Phys. Rev. B **83**, 205101 (2011).
[2] P. Hosur and X. Qi, C.R. Phys. **14**, 857 (2013).
[3] A. Burkov, J. Phys. Condens. Matter **27**, 113201 (2015).
[4] H.-J. Kim, K.-S. Kim, J.-F. Wang, M. Sasaki, N. Satoh, A. Ohnishi, M. Kitaura, M. Yang, and L. Li, Phys. Rev. Lett. **111**, 246603 (2013).
[5] S.-Y. Xu, I. Belopolski, N. Alidoust, M. Neupane, G. Bian, C. Zhang, R. Sankar, G. Chang, Z. Yuan, C.-C. Lee, S.-M. Huang, H. Zheng, J. Ma, D. S. Sanchez, B. Wang, A. Bansil, F. Chou, P. P. Shibayev, H. Lin, S. Jia, and M. Z. Hasan, Science **349**, 613 (2015).
[6] S.-Y. Xu, N. Alidoust, I. Belopolski, Z. Yuan, G. Bian, T.-R. Chang, H. Zheng, V. N. Strocov, D. S. Sanchez, G. Chang, C. Zhang, D. Mou, Y. Wu, L. Huang, C.-C. Lee, S.-M. Huang, B.-K. Wang, A. Bansil, H.-T. Jeng, T. Neupert, A. Kaminski, H. Lin, S. Jia, and M. Z. Hasan, Nat. Phys. **11**, 748 (2015).
[7] X. Huang, L. Zhao, Y. Long, P. Wang, D. Chen, Z. Yang, H. Liang, M. Xue, H. Weng, Z. Fang, X. Dai, and G. Chen, Phys. Rev. X **5**, 031023 (2015).
[8] S.-M. Huang, S.-Y. Xu, I. Belopolski, C.-C. Lee, G. Chang, B. Wang, N. Alidoust, G. Bian, M. Neupane, C. Zhang, S. Jia, A. Bansil, H. Lin, and M. Z. Hasan, Nat. Commun. **6**, 7373 (2015).
[9] C. Shekhar, A. K. Nayak, Y. Sun, M. Schmidt, M. Nicklas, I. Leermakers, U. Zeitler, Y. Skourski, J. Wosnitza, Z. Liu, Y. Chen, W. Schnelle, H. Borrmann, Y. Grin, C. Felser, and B. Yan, Nat. Phys. **11**, 645 (2015).
[10] B. Q. Lv, N. Xu, H. M. Weng, J. Z. Ma, P. Richard, X. C. Huang, L. X. Zhao, G. F. Chen, C. E. Matt, F. Bisti, V. N. Strocov, J. Mesot, Z. Fang, X. Dai, T. Qian, M. Shiand, and H. Ding, Nat. Phys. **11**, 724 (2015).
[11] L. X. Yang, Z. K. Liu, Y. Sun, H. Peng, H. F. Yang, T. Zhang, B. Zhou, Y. Zhang, Y. F. Guo, M. Rahn, D. Prabhakaran, Z. Hussain, S.-K. Mo, C. Felser, B. Yan, and Y. L. Chen, Nat. Phys. **11**, 728 (2015).
[12] J. Xiong, S. K. Kushwaha, T. Liang, J. W. Krizan, M. Hirschberger, W. Wang, R. Cava, and N. Ong, Science **350**, 413 (2015).
[13] C.-L. Zhang, S.-Y. Xu, I. Belopolski, Z. Yuan, Z. Lin, B. Tong, G. Bian, N. Alidoust, C.-C. Lee, S.-M. Huang, T.-R. Chang, G. CHang, C.-H. Hsu, H.-T. Jeng, M. Neupane, D. S. Sanchez, H. Zheng J. Wang, H. Lin, C. Zhang, H.-Z. Lu, S.-Q. Shen, T. Neupert, M. Z. Hasan, and S. Jia, Nat. Commun. **7**, 10735 (2016).
[14] H. Nielsen and M. Ninomiya, Phys. Lett. B **130**, 389 (1983).
[15] K. Fukushima, D. E. Kharzeev, and H. J. Warringa, Phys. Rev. D **78**, 074033 (2008).
[16] A. A. Zyuzin and A. A. Burkov, Phys. Rev. B **86**, 115133 (2012).
[17] V. Aji, Phys. Rev. B **85**, 241101 (2012).
[18] D. T. Son and B. Z. Spivak, Phys. Rev. B **88**, 104412 (2013).
[19] A. A. Burkov, Phys. Rev. Lett. **113**, 247203 (2014).
[20] S. A. Parameswaran, T. Grover, D. A. Abanin, D. A. Pesin, and A. Vishwanath, Phys. Rev. X **4**, 031035 (2014).
[21] E. V. Gorbar, V. A. Miransky, and I. A. Shovkovy, Phys. Rev. B **89**, 085126 (2014).
[22] B. Sbierski, G. Pohl, E. J. Bergholtz, and P. W. Brouwer, Phys. Rev. Lett. **113**, 026602 (2014).
[23] J. Klier, I. V. Gornyi, and A. D. Mirlin, Phys. Rev. B **92**, 205113 (2015).
[24] P. Hosur, S. A. Parameswaran, and A. Vishwanath, Phys. Rev. Lett. **108**, 046602 (2012).
[25] A. Altland and D. Bagrets, Phys. Rev. B **93**, 075113 (2016).
[26] P. Baireuther, J. A. Hutasoit, J. Tworzydo, and C. W. J. Beenakker, New J. Phys. **18**, 045009 (2016).
[27] In relatively narrow WSM samples, surface states may provide a significant contribution to transport. This is particularly relevant when the Landau level degeneracy m is of order one. However, such a contribution can be avoided if the magnetic field is oriented parallel to the separation between Weyl nodes of opposite chirality.
[28] M. Grayson, D. Schuh, M. Huber, M. Bichler, and G. Abstreiter, Appl. Phys. Lett. **86**, 032101 (2005).
[29] M. Grayson, L. Steinke, D. Schuh, M. Bichler, L. Hoeppel, J. Smet, K. v. Klitzing, D. Maude, and G. Abstreiter, Phys. Rev. B **76**, 201304 (2007).
[30] M. Grayson, L. Steinke, M. Huber, D. Schuh, M. Bichler, and G. Abstreiter, Phys. Status Solidi B **245**, 356 (2008).
[31] L. Steinke, D. Schuh, M. Bichler, G. Abstreiter, and M. Grayson, Phys. Rev. B **77**, 235319 (2008).
[32] E. Khalaf, M. A. Skvortsov, and P. M. Ostrovsky, Phys. Rev. B **93**, 125405 (2016).
[33] K. Wakabayashi, Y. Takane, and M. Sigrist, Phys. Rev. Lett. **99**, 036601 (2007).

[34] O. Dorokhov, Solid State Commun. **51**, 381 (1984).
[35] Y. V. Nazarov, Phys. Rev. Lett. **73**, 134 (1994).
[36] H. Lee, L. S. Levitov, and A. Y. Yakovets, Phys. Rev. B **51**, 4079 (1995).
[37] Y. V. Nazarov and Y. M. Blanter, *Quantum Transport: Introduction to Nanoscience* (Cambridge University Press, Cambridge, England, 2009).
[38] K. Efetov and A. Larkin, Sov. Phys. JETP **58**, 444 (1983).
[39] K. Efetov, *Supersymmetry in Disorder and Chaos* (Cambridge University Press, Cambridge, England, 1999).
[40] A. D. Mirlin, Phys. Rep. **326**, 259 (2000).
[41] A. M. Pruisken, Nucl. Phys. **B235**, 277 (1984).
[42] J. Wess and B. Zumino, Phys. Lett. B **37**, 95 (1971).
[43] E. Witten, Nucl. Phys. **B223**, 422 (1983).
[44] E. Witten, Commun. Math. Phys. **92**, 455 (1984).
[45] B. Rejaei, Phys. Rev. B **53**, R13235 (1996).
[46] See Supplemental Material at http://link.aps.org/supplemental/10.1103/PhysRevLett.119.106601 for a detailed derivation and analysis of the non-linear sigma model and the corresponding transfer matrix Hamiltonian for the matrix Green's function in the presence of chiral channels.
[47] C. W. Beenakker, Rev. Mod. Phys. **69**, 731 (1997).
[48] R. P. Feynman and A. R. Hibbs, *Quantum Mechanics and Path Integrals* (McGraw-Hill, New York, 1965).
[49] B. Sutherland, Phys. Rev. A **5**, 1372 (1972).
[50] M. R. Zirnbauer, Phys. Rev. Lett. **69**, 1584 (1992).
[51] A. D. Mirlin, A. Mullergroeling, and M. R. Zirnbauer, Ann. Phys. (N.Y.) **236**, 325 (1994).
[52] K. Frahm, Phys. Rev. Lett. **74**, 4706 (1995).
[53] A. Lamacraft, B. D. Simons, and M. R. Zirnbauer, Phys. Rev. B **70**, 075412 (2004).
[54] F. Evers and A. D. Mirlin, Rev. Mod. Phys. **80**, 1355 (2008).
[55] Both internode and intranode scattering rates enter our formalism as parameters and they may, in principle, depend on a magnetic field. However, such dependence will be most pronounced in strong enough fields close to the clean ultraquantum limit and will not be important for the fields we are considering, when many Landau levels intersect the Fermi surface.